SCIENCE CHINA
Physics, Mechanics & Astronomy

• Research Paper •

October 2011 Vol.54 No.10: 1883–1888
doi: 10.1007/s11433-011-4454-2

Numerical study of detonation shock dynamics using generalized finite difference method

CHEN YongLi, HUANG KuiBang & YU Xin*

Institute of Applied Physics and Computational Mathematics, Beijing 100094, China

Received April 26, 2011; accepted July 8, 2011; published online August 30, 2011

The generalized finite difference method (GFDM) used for irregular grids is first introduced into the numerical study of the level set equation, which is coupled with the theory of detonation shock dynamics (DSD) describing the propagation of the detonation shock front. The numerical results of a rate-stick problem, a converging channel problem and an arc channel problem for specified boundaries show that GFDM is effective on solving the level set equation in the irregular geometrical domain. The arrival time and the normal velocity distribution of the detonation shock front of these problems can then be obtained conveniently with this method. The numerical results also confirm that when there is a curvature effect, the theory of DSD must be considered for the propagation of detonation shock surface, while classic Huygens construction is not suitable any more.

generalized finite difference method, detonation shock dynamics, level set equation, propagation of detonation shock front, irregular grids

PACS: 47.40.Rs, 02.70.Bf, 02.60.Cb

1 Introduction

The level set method combined with the theory of detonation shock dynamics (DSD) is now widely used to study the non-ideal propagation of detonation shock front. The theory of DSD was mainly proposed and developed by Bdzil and Stewart and their colleagues based on an asymptotic theory [1–3]. The main conclusion of DSD is when the curvature radius of the curved shock is large compared with the width of the reaction zone of the corresponding explosive, the normal velocity of the detonation shock front equals the plane CJ velocity plus a correction caused by the local curvature of the front, i.e.

$$D_n(\kappa) = D_{\mathrm{CJ}} - \alpha(\kappa), \tag{1}$$

where D_n is the normal velocity of the detonation shock front, D_{CJ} is the steady CJ velocity of one-dimensional detonation, and $\alpha(\kappa)$ is a function of the detonation front curvature determined by the properties of the explosive. From the derivation of D_n-κ relation [3,4], one can know that the relation depends on the chemical dynamics proceeding in the reaction zone, and the relation is an intrinsic property of the corresponding explosive. Provided that the initial shape of the shock front, the D_n-κ relation and the boundary conditions are given, an initial-boundary value problem of the propagation of the detonation shock front can be defined, with no need to solve the reactive compressive flow in a real reaction zone.

The level set method for the DSD theory was first proposed by Aslam et al. [5] in Cartesian coordinates. This method embeds the propagating detonation front in a space of one higher dimension, and then evolves the front automatically according to a level set equation, while other methods based on surface parameterization require boring logic to solve the problems of front merging and bifurcation.

*Corresponding author (email: yummuy@iapcm.ac.cn)

Wen [6], Chen et al. [7], and Zhong [8] studied the non-ideal propagation of the detonation shock front adopting the level set method and the DSD theory, respectively. Chen et al. [7] used the body-fitted coordinates to simplify the handling of boundary conditions. Zhong [8] then investigated the finite difference scheme of the level set equation in the three- dimensional non-orthogonal body-fitted coordinates. One should note that it is very complicated to deal with the boundary conditions by using rectangular grids in Cartesian coordinates as Aslam et al. [5] and Wen [6] did in their work, where the computational grid points are not exactly on the boundary of the explosive. The finite difference method in body-fitted coordinates has some inherent limitations, such as a higher requirement for the grid quality and the so-called geometry induced error.

A generalized finite difference method (GFDM) for irregular grids proposed by Liszka & Orkisz [9,10] keeps the implementary simplicity of traditional finite difference method without increasing the computational cost when it is used to solve second order partial differential equations. Recently, Gavete et al. [11,12] made a comprehensive study of GFDM and compared the numerical precision of GFDM with that of element free Galerkin method, and the convergence, the truncation errors over irregular grids and the stability criterion of the method for parabolic and hyperbolic equations were investigated there. Prieto et al. [13] described how GFDM could be applied for solving the advection-diffusion equation, as well as its corresponding analysis. The related research reports above show that GFDM is good at numerically solving partial differential equations for irregular grids in complicated areas.

In this paper, we will study numerically the level set equation coupled with the DSD theory using GFDM for trapeziform grids in Cartesian coordinates in the complicated computational region, which is the basis of our further research on the propagation problem of the curved detonation shock front.

2 Computational method

2.1 Control equation

The level set technique looks for a field function $\psi(\boldsymbol{x}, t)$ in a space that the surface of interest travels in, and the zero constant iso-surface $\psi(\boldsymbol{x}, t)=0$ is often defined to be the appropriate one. For a level surface $\psi(\boldsymbol{x}, t)$=const, its total derivative is zero, i.e. [5]

$$\frac{\mathrm{d}\psi}{\mathrm{d}t}=\frac{\partial\psi}{\partial t}+\boldsymbol{D}(\kappa)\cdot\nabla\psi=0, \tag{2}$$

where $\boldsymbol{D}(\kappa)$ is the surface velocity related to its total curvature κ. Since the detonation front propagates along its normal direction only, i.e. $\boldsymbol{D}(\kappa)=D_n(\kappa)\boldsymbol{n}_s$, where $\boldsymbol{n}_s$ is the outward unit normal vector of the front, eq. (2) can be written in the following form:

$$\frac{\partial\psi}{\partial t}+D_n(\kappa)\left|\nabla\psi\right|=0, \tag{3}$$

where the normal is given by $\boldsymbol{n}_s=\nabla\psi/\left|\nabla\psi\right|$ in terms of the level set function. Substituting eq. (1) into eq. (3), we can get the following control equation:

$$\frac{\partial\psi}{\partial t}+D_{\mathrm{CJ}}\left|\nabla\psi\right|-\alpha(\kappa)\left|\nabla\psi\right|=0. \tag{4}$$

This is the level set equation describing the propagation of the detonation shock front. The total curvature of the front in the two-dimensional space is as follows:

$$\kappa=\nabla\cdot\boldsymbol{n}_s=\nabla\cdot\left(\frac{\nabla\psi}{\left|\nabla\psi\right|}\right)=\frac{\psi_{xx}\psi_y^2-2\psi_x\psi_y\psi_{xy}+\psi_{yy}\psi_x^2}{\left(\psi_x^2+\psi_y^2\right)^{3/2}}. \tag{5}$$

Especially, if a linear D_n-κ relation is applied, i.e. $D_n(\kappa)=D_{\mathrm{CJ}}-a\kappa$, then eq. (4) reads

$$\frac{\partial\psi}{\partial t}+D_{\mathrm{CJ}}\left|\nabla\psi\right|-a\kappa\left|\nabla\psi\right|=0, \tag{6}$$

where a is a constant coefficient. When expression (5) is substituted into eq. (6), the following partial differential equation can be obtained

$$\begin{aligned}&\frac{\partial\psi}{\partial t}+D_{\mathrm{CJ}}\left(\psi_x^2+\psi_y^2\right)^{1/2}\\&-a\frac{\psi_{xx}\psi_y^2-2\psi_x\psi_y\psi_{xy}+\psi_{yy}\psi_x^2}{\psi_x^2+\psi_y^2}=0.\end{aligned} \tag{7}$$

Eq. (7) is the very level set equation coupled with a linear relation of the DSD theory in the two-dimensional space, which is to be numerically solved in this paper.

For eq. (7), a first order forward Euler differencing is used for the time derivative:

$$\frac{\partial\psi}{\partial t}=\frac{\psi_{i,j}^{n+1}-\psi_{i,j}^{n}}{\Delta t}, \tag{8}$$

where i and j denote the x and y nodes, and n, the time level, respectively. The discrete scheme for the time derivative used here is first order accurate and higher order schemes such as the Runge-Kutta method will be employed if it is necessary in our further studies. The first and second order spatial derivatives appearing in eq. (7) are calculated using the GFD scheme introduced in sect. 1, of which some numerical details will be given in sect. 2.3.

2.2 Boundary conditions

The boundary condition depends on the flow type observed by a viewer riding on the intersection of the shock front and the edge, and the flow type is characterized by the local sonic parameter [5]:

$$S \equiv C^2 - U_n^2 - D_n^2 \cot^2(\omega), \tag{9}$$

where S is the local sonic parameter, C, the sound speed in the explosive, U_n, the particle velocity of the explosive in the shock-normal direction, D_n, the normal velocity of the detonation shock front, and ω is the angle between the local shock normal $\boldsymbol{n}_s$ and the normal vector of the edge $\boldsymbol{n}_b$. Figure 1 shows a schematic diagram of the definition of angle ω, and the normals $\boldsymbol{n}_s$ and $\boldsymbol{n}_b$. It is clear that

$$\cos\omega = \boldsymbol{n}_s \cdot \boldsymbol{n}_b. \tag{10}$$

Eq. (10) is just the so-called angle boundary condition.

When S<0, the flow is locally supersonic at the intersection of the shock front and the edge and there is no need to apply a boundary condition. In this case, a continuation boundary condition is used in the numerical implementation. When S=0, the flow is locally sonic and the angle becomes $\omega=\omega_s$, which is a constant sonic angle determined by the equation of state of the explosive. In this case, if the confinement is considerably weak, the flow at the shock/edge intersection point will remain sonic and the angle will stay as ω_s. But if the confinement is very heavy, the local flow will experience a rapid transition to subsonic flow (S>0) and the angle becomes $\omega=\omega_c>\omega_s$, where ω_c is the angle where the pressure in the explosive and the pressure in the inert reach an equilibrium value. The angle ω_c is regarded as a material constant depending on the properties of the explosive/inert pair only, and it can be obtained by an experiment or a shock polar analysis. The applied angle boundary condition is also related to the initial shape of the shock front, and further details can be found in ref. [5].

In our study, the edge normal vector $\boldsymbol{n}_b$ is easily known by some interpolation scheme such as Hermite interpolation in case that the coordinates of those boundary nodes are given. The shock normal vector is directly calculated by the level set function, $\boldsymbol{n}_s = \nabla\psi / |\nabla\psi|$, but the level set function values of those nodes outside the explosive boundary are unknown and should be determined by the angle boundary condition, i.e. eq. (10), which can be rewritten as follows:

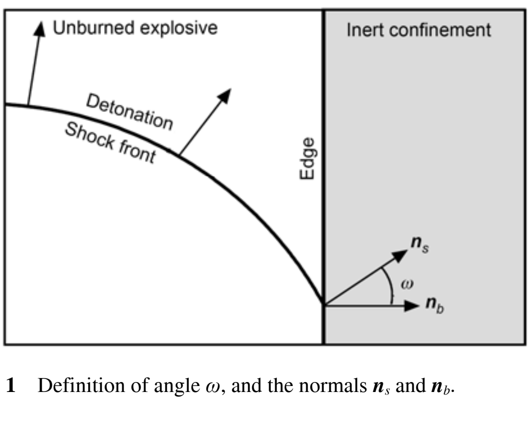

Figure 1 Definition of angle ω, and the normals $\boldsymbol{n}_s$ and $\boldsymbol{n}_b$.

$$\cos\omega = \frac{(\partial\psi/\partial x)n_{bx} + (\partial\psi/\partial y)n_{by}}{\sqrt{(\partial\psi/\partial x)^2 + (\partial\psi/\partial y)^2}}, \tag{11}$$

where n_{bx} and n_{by} are the respective components of $\boldsymbol{n}_b$ in two-dimensional space. Take Figure 2 for example, where nodes P_0, P_1 and P_3 are at the edge, and P_2 is located in the confinement, and P_4 is in the explosive. When the level set function evolves according to eq. (7), $\psi(P_2)$ is unknown. We apply the following Green formula in the domain surrounded by dashed lines in Figure 2:

$$\nabla\psi \approx \frac{\oint \psi \boldsymbol{n} \mathrm{d}l}{\iint \mathrm{d}x\mathrm{d}y}, \tag{12}$$

i.e.

$$\frac{\partial\psi}{\partial x} \approx \frac{\oint \psi \mathrm{d}y}{\iint \mathrm{d}x\mathrm{d}y}, \quad \frac{\partial\psi}{\partial y} \approx -\frac{\oint \psi \mathrm{d}x}{\iint \mathrm{d}x\mathrm{d}y}. \tag{13}$$

A central scheme is used and then the discrete forms of $\partial\psi/\partial x$ and $\partial\psi/\partial y$ can be obtained as functions of $\psi(P_i)$, $i = 1,\cdots,4$, among which $\psi(P_2)$ is unknown. Substituting the discrete forms of $\partial\psi/\partial x$ and $\partial\psi/\partial y$ into expression (11), one gets a nonlinear algebraic equation with an unknown quantity $\psi(P_2)$, which can be solved using some iterative method or other numerical methods. Once the level set function values of all the nodes outside the explosive edge such as $\psi(P_2)$ are determined, the field function $\psi(\boldsymbol{x}, t)$ can evolve according to eq. (7) in the whole computational domain.

2.3 GFD scheme of spatial derivatives

The generalized finite difference method is actually one of the meshless methods [9,10]. Using GFDM in this paper is to solve nonlinear partial differential eq. (7) for irregular

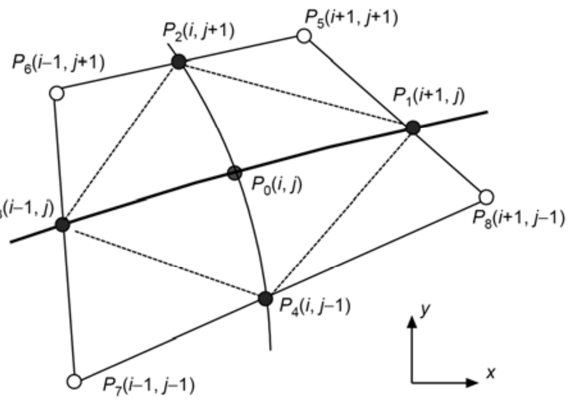

Figure 2 A schematic diagram of nodes inside, outside or at the edge of the explosive, where nodes P_0, P_1 and P_3 are at the edge, and P_2 is in the confinement, P_4 in the explosive.

grids numerically. The GFD scheme for all spatial derivatives of the level set function $\psi(\boldsymbol{x}, t)$ appearing in eq. (7) is as follows.

For the level set function at time t^n in a given two-dimensional domain, expression $\psi(\boldsymbol{x}, t)=\psi(x, y, t^n)=\psi^n(x, y)$ holds. We ignore the superscript n of $\psi^n(x, y)$ and mark it as $\psi(x, y)$ for convenience in the following paragraphs. If a central node $P(x_0, y_0)$ and its neighboring nodes are defined, then according to the Taylor series expansion around node P we know that

$$\psi_i=\psi_0+h_i\frac{\partial\psi_0}{\partial x}+k_i\frac{\partial\psi_0}{\partial y}+\frac{h_i^2}{2}\frac{\partial^2\psi_0}{\partial x^2}+\frac{k_i^2}{2}\frac{\partial^2\psi_0}{\partial y^2}+k_ih_i\frac{\partial^2\psi_0}{\partial x\partial y}+O(\Delta^3),\quad i=1,\cdots,m, \tag{14}$$

where $\psi_i=\psi(x_i, y_i)$, $\psi_0=\psi(x_0, y_0)$, $h_i=x_i-x_0$, $k_i=y_i-y_0$, $\Delta=\sqrt{h_i^2+k_i^2}$, and m ($m\geqslant 5$) is the number of neighbor nodes. We can then obtain a set of linear equations by ignoring the higher order terms $O(\Delta^3)$,

$$\boldsymbol{A}\cdot\{D\psi\}=\{\psi\}, \tag{15}$$

with

$$\boldsymbol{A}=\begin{bmatrix} h_1 & k_1 & h_1^2/2 & k_1^2/2 & h_1k_1 \\ h_2 & \cdots & \cdots & \cdots & h_2k_2 \\ \vdots & & & & \vdots \\ h_m & \cdots & \cdots & \cdots & h_mk_m \end{bmatrix}, \tag{16a}$$

$$\{\psi\}^{\mathrm{T}}=\{\psi_1-\psi_0,\psi_2-\psi_0,\cdots,\psi_m-\psi_0\}, \tag{16b}$$

$$\{D\psi\}^{\mathrm{T}}=\left\{\frac{\partial\psi_0}{\partial x},\frac{\partial\psi_0}{\partial y},\frac{\partial^2\psi_0}{\partial x^2},\frac{\partial^2\psi_0}{\partial y^2},\frac{\partial^2\psi_0}{\partial x\partial y}\right\}, \tag{16c}$$

where $\{D\psi\}$ is a vector composed of five unknown spatial derivatives at the central node $P(x_0, y_0)$. The minimum number of neighboring nodes is m=5 to determine the $\{D\psi\}$ vector, and the number should be increased in order to improve the accuracy in approximating the derivatives leading to an overdetermined set of equations. In that case, the solution may be obtained by the least square procedure by considering the minimization of the norm:

$$B=\sum_{i=1}^{m}\left[\left(\psi_0-\psi_i+\frac{\partial\psi_0}{\partial x}h_i+\frac{\partial\psi_0}{\partial y}k_i+\frac{\partial^2\psi_0}{\partial x^2}\frac{h_i^2}{2}+\frac{\partial^2\psi_0}{\partial y^2}\frac{k_i^2}{2}+\frac{\partial^2\psi_0}{\partial x\partial y}k_ih_i\right)w_i\right]^2=\min, \tag{17}$$

and $w_i=w_i(h_i,k_i)$ are weighting functions. The necessary conditions satisfying eq. (17) are

$$\frac{\partial B}{\partial\{D\psi\}}=0. \tag{18}$$

Then a set of five linear equations with five unknown spatial derivatives emerge as:

$$\boldsymbol{A}\cdot\{D\psi\}=\boldsymbol{b}, \tag{19}$$

with

$$\boldsymbol{A}=\begin{bmatrix}
\sum_{i=1}^m w_i^2h_i^2 & \sum_{i=1}^m w_i^2h_ik_i & \sum_{i=1}^m w_i^2h_i^3/2 & \sum_{i=1}^m w_i^2h_ik_i^2/2 & \sum_{i=1}^m w_i^2h_i^2k_i \\
\sum_{i=1}^m w_i^2h_ik_i & \sum_{i=1}^m w_i^2k_i^2 & \sum_{i=1}^m w_i^2h_i^2k_i/2 & \sum_{i=1}^m w_i^2k_i^3/2 & \sum_{i=1}^m w_i^2h_ik_i^2 \\
\sum_{i=1}^m w_i^2h_i^3/2 & \sum_{i=1}^m w_i^2h_i^2k_i/2 & \sum_{i=1}^m w_i^2h_i^4/4 & \sum_{i=1}^m w_i^2h_i^2k_i^2/4 & \sum_{i=1}^m w_i^2h_i^3k_i/2 \\
\sum_{i=1}^m w_i^2h_ik_i^2/2 & \sum_{i=1}^m w_i^2k_i^3/2 & \sum_{i=1}^m w_i^2h_i^2k_i^2/4 & \sum_{i=1}^m w_i^2k_i^4/4 & \sum_{i=1}^m w_i^2h_ik_i^3/2 \\
\sum_{i=1}^m w_i^2h_i^2k_i & \sum_{i=1}^m w_i^2h_ik_i^2 & \sum_{i=1}^m w_i^2h_i^3k_i/2 & \sum_{i=1}^m w_i^2h_ik_i^3/2 & \sum_{i=1}^m w_i^2h_i^2k_i^2
\end{bmatrix}, \tag{19a}$$

$$\boldsymbol{b}=\begin{bmatrix}
\sum_{i=1}^m w_i^2h_i\left(\psi_i-\psi_0\right) \\
\sum_{i=1}^m w_i^2k_i\left(\psi_i-\psi_0\right) \\
\sum_{i=1}^m w_i^2h_i^2\left(\psi_i-\psi_0\right)/2 \\
\sum_{i=1}^m w_i^2k_i^2\left(\psi_i-\psi_0\right)/2 \\
\sum_{i=1}^m w_i^2h_ik_i\left(\psi_i-\psi_0\right)
\end{bmatrix}. \tag{19b}$$

Because the matrix of coefficient $\boldsymbol{A}$ is symmetrical, it is easy to solve eq. (19) using the Cholesky method [11,12].

In the following numerical examples, structured irregular quadrangles are adopted and a nine nodes stencil is used, i.e. a central node surrounded by eight neighboring nodes (m=8). The weighting functions $w_i(h_i, k_i)$ appearing in eqs. (19a) and (19b) are all taken as 1 in this paper. Figure 2 gives a schematic display of the stencil, and P_0 represents the node located either in the computational domain or at the edge here.

3 Numerical examples

3.1 Rate stick problem

As shown in Figure 3, the computational domain is $(x, y)\in$ [0, 200 mm]×[0, 40 mm] and the grid is 200×40, $\Delta x=\Delta y$=1 mm. The obtained cells are regular rectangular quadrangles in this case. A plane wave is initially located at x=5 mm, and the level set function is initially a signed distance function from the wave front leading to $\psi(x>5\text{ mm})>0$, $\psi(x=5\text{ mm})=0$, $\psi(x<5\text{ mm})<0$. Symmetric boundary condition which is in accordance with perfect confinement is applied at y=0, and the angle boundary condition, ω_c=54.7°, is applied at y=40 mm. At x=0 and x=200 mm, continuation boundary conditions are adopted.

In the evolution of $\psi(x, y, t)$ based on eq. (7) in the whole field, for a specified node, the time at which the level set function value change sign is recorded as the arrival time of the shock front. Figure 3 shows the detonation shock fronts at times t=0.5, 4, 8, 12, 16, 20, 24 μs, respectively, which are obtained by the DSD theory with D_n-κ relation given by $D_n(\kappa)=(8.0-50.8\kappa)$ mm/μs. From Figure 3, one can see that the shock fronts at the edge y=40 mm are curved and slowed gradually due to the angle boundary condition. In addition, the shock fronts at corresponding times given by Huygens construction are plotted in Figure 3, and the Huygens solutions with constant propagating velocity D_n=8.0 mm/μs are evidently not able to predict the curvature effect at the boundary. From the normal velocity distribution of the detonation shock front, marked by $D_n(x, y)$, one can find that the detonation velocity near the upper boundary is smaller than that close to the central line.

3.2 Converging channel problem

In this case, the computational domain is a converging channel as shown in Figure 4. The length in the x direction is 200 mm, and the lengths in the y direction are 100 and 60 mm on the left and right sides, respectively, where there is a flat part on the left side with length 20 mm. The gird applied in the numerical simulation is 200×100, leading to regular rectangular cells in the flat part and irregular quadrangles in the converging part. An initial plane wave is located at x=5 mm and the level set function is initially a signed distance function from the wave front. Symmetric condition and the angle boundary condition with ω_c=90° are used at the bottom and top boundaries, respectively, and continuation conditions are applied at x=0 and x=200 mm.

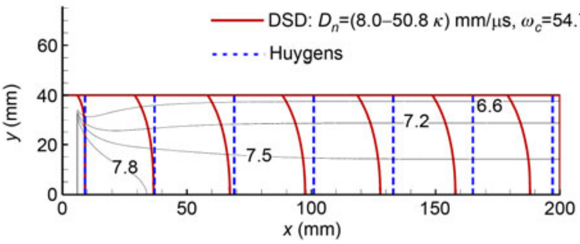

Figure 3 (Color online) Propagation process of the detonation shock front in a rate stick problem: the thick solid lines denote the shock fronts of level set solutions to the DSD theory at times t=0.5, 4, 8, 12, 16, 20, 24 μs, respectively, the thick dashed lines denote the corresponding solutions of Huygens construction, and the thin solid lines denote the distribution of normal velocity of the detonation shock front, i.e. $D_n(x,y)$.

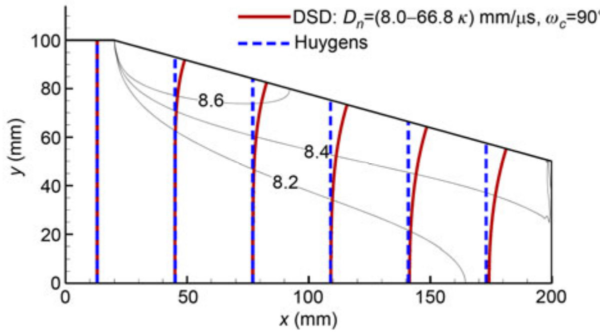

Figure 4 (Color online) Propagation process of the detonation shock front in a converging channel problem: the thick solid lines denote the shock fronts of level set solutions to the DSD theory at times t=1, 5, 9, 13, 17, 21 μs, respectively, the thick dashed lines denote the corresponding solutions of Huygens construction, and the thin solid lines denote the distribution of normal velocity of the detonation shock front, i.e. $D_n(x,y)$.

Figure 4 shows the locations of the detonation shock front at times t=1, 5, 9, 13, 17, 21 μs, respectively, obtained by the simulation of the level set equation together with the DSD theory with $D_n=(8.0-66.8\kappa)$ mm/μs, which is cited from references [4,5] and is derived from the reactive compressive Euler equations with a simplified rate law of $r=2.5147(1-\lambda)^{1/2}$ μs^{-1}, where λ is the reaction progress variable. One can find that the shock fronts are curved and accelerated at the top edge of the converging part because of the negative curvature there. However, the solutions to Huygens construction with constant propagating velocity D_n=8.0 mm/μs are slower and slower than the numerical results of the DSD theory. One can also find that the normal velocity in the vicinity of the top boundary is bigger than that close to the central line from the normal velocity distribution of the detonation shock front.

3.3 Arc channel problem

The computational domain of the arc channel problem is

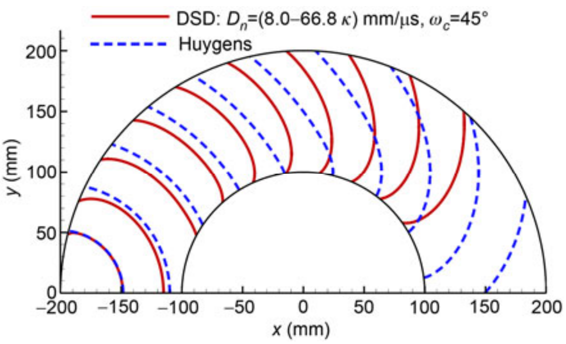

Figure 5 (Color online) Propagation process of the detonation shock front in an arc channel problem: the thick solid lines denote the shock fronts of level set solutions to the DSD theory at times t=0.2, 5, 10, 15, 20, 25, 30, 35, 40, 45 μs, respectively, and the thick dashed lines denote the corresponding solutions of Huygens construction.

shown in Figure 5, where the inner radius and the outer radius are 100 and 200 mm, respectively. The grid in the simulation is 100×360 in the radial and in the circular directions, respectively. The initial detonation front is an arc centered at (−200 mm, 0) with radius R_0=50 mm and again a signed distance function from the initial front is prepared for the initial level set function in the whole domain. Both the inside and outside boundaries of the arc channel use the angle boundary condition, i.e. the sonic angle ω_s=45° corresponding to free confinement or very light confinement. The applied D_n-κ relation is given by D_n=(8.0–66.8κ) mm/μs.

The detonation shock fronts at times t=0.2, 5, 10, 15, 20, 25, 30, 35, 40, 45 μs, respectively, given by the simulation of the DSD theory are shown in Figure 5. The distribution of the normal velocity of the shock fronts is not plotted here in order to show the front locations clearly. One can observe that the shock fronts obtained by the DSD theory lag behind those predicted by Huygens construction quickly with the specified computational conditions. The discrepancies of the results at later times between the DSD theory and Huygens construction are so large that one must consider the curvature effect in this case, and thus the arrival time of the detonation shock front used in traditional algorithms for detonation simulations of the explosives should be improved by applying the DSD theory.

4 Conclusions

In this paper, GFDM is successfully applied to solve the level set equation that is combined with the DSD theory numerically for irregular quadrangular grids, and then the propagation time of the detonation shock front and the distribution of the normal velocity of the shock front in complex explosive devices can be obtained conveniently.

The simulations of detonation shock front propagating in the examples of a rate stick, a converging channel and an arc channel show that the traditional Huygens construction is not suitable for calculating the propagation of shock front any more when the front is curved, while a more accurate theory must be developed such as the theory of DSD, especially at the edge of the explosives.

However, the optimization of the numerical algorithm used in this paper and more detailed investigations of the propagation of detonation shock front in those engineering problems need to be carried out in the following work. Moreover, partial differential eq. (4) or eq. (7) solved in this paper is quite nonlinear, and there have been few studies about the mathematical properties of GFDM for a nonlinear partial differential equation to our knowledge. Therefore, a rigorous analysis of the convergence and the truncation error of the numerical method adopted here is also an essential study to be done in the future.

The comments of the anonymous reviewers are gratefully acknowledged. This work was supported by the National Natural Science Foundation of China (Grant No. 11002029).

1 Bdzil J B, Stewart D S. The dynamics of detonation in explosive systems. Annu Rev Fluid Mech, 2007, 39: 263–292
2 Stewart D S, Bdzil J B. The shock dynamics of stable multidimensional detonation. Combust Flame, 1988, 72: 311–323
3 Bdzil J B, Stewart D S. Modeling two-dimensional detonations with detonation shock dynamics. Phys Fluids A, 1989, 1: 1261–1267
4 Yao J, Stewart D S. On the dynamics of multi-dimensional detonation. J Fluid Mech, 1996, 309: 225–275
5 Aslam T D, Bdzil J B, Stewart D S. Level Set methods applied to modeling detonation shock dynamics. J Comput Phys, 1996, 126: 390–409
6 Wen S G. The LS Method Applied to Three Dimensional Detonation Wave Propagation. Dissertation for the Doctoral Degree. China Acad Eng Phys, 2001
7 Chen S H, Zhang X, Bo J S. LS method in body-fitted coordinate system for multi-dimensional non-ideal detonation propagation. Chin J High Pressure Phys, 2000, 14: 280–284
8 Zhong M. The Numerical Method and Simulation for Propagating Front of Non-ideal 3D Detonation. Dissertation for the Master Degree. China Acad Eng Phys, 2005
9 Liszka T, Orkisz J. The finite difference method at arbitrary irregular grids and its application in applied mechanics. Comput Struct, 1980, 11: 83–95
10 Orkisz J. Finite difference method (Part III). Kleiber M, ed. Handbook of Computational Solid Mechanics Survey and Comparison of Contemporary Methods. Berlin: Springer, 1998
11 Gavete L, Gavete M L, Benito J J. Improvements of generalized finite difference method and comparison with other meshless method. Appl Math Model, 2003, 27: 831–847
12 Benito J J, Urena F, Gavete L. Solving parabolic and hyperbolic equations by generalized finite difference method. J Comput Appl Math, 2007, 209: 208–233
13 Prieto F U, Benito Munoz J J, Corvinos L G. Application of the generalized finite difference method to solve the advection-diffusion equation. J Comput Appl Math, 2011, 235: 1849–1855